Research Article

Amjad Ibrahim Oraibi, Ashour H. Dawood, Nawres Debbabi, Ali Majeed Ali Almukram, Khalid S. Almaary*, Fakhreldeen Dabiellil*, Leila Chekir-Ghedira, Soumaya Kilani-Jaziri

Resveratrol-derived MDM2 inhibitors: Synthesis, characterization, and biological evaluation against MDM2 and HCT-116 cells

https://doi.org/10.1515/chem-2025-0142 received October 4, 2024; accepted March 11, 2025

Abstract: This study investigates the biological potential of novel resveratrol-based derivatives targeting the MDM2 protein, a critical regulator of the tumour suppressor p53 in cancer therapy. We synthesized and characterized four derivatives of (*E*)-2,4-dimethoxy-6-(4-methoxystyryl) benzaldehyde using mass spectrometry, proton nuclear magnetic resonance, and Fourier-transform infrared spectroscopy. These derivatives were specifically designed to enhance binding affinity, stability, and selectivity compared to inhibitors like Nutlin. Biological evaluation through MTT assays revealed varying antiproliferative activities against HCT-116 cancer cells. AMJ3 exhibited the strongest activity, with an IC50 value of 22.69 ±

2.47 µg/mL, outperforming that of the reference compound Nutlin (IC50: 62.72 \pm 3.15 µg/mL). MDM2-p53 inhibitory activity confirmed AMJ3 as the most potent inhibitor (IC50: 0.24 \pm 0.02 µM), followed by AMJ5 (IC50: 0.48 \pm 0.04 µM), both surpassing Nutlin (IC50: 0.39 \pm 0.03 µM). Molecular docking studies for AMJ3 and AMJ6 achieved superior glide scores of –5.6 and –4.9, respectively. Molecular dynamics simulations validated these findings, showing that AMJ3 formed a stable hydrogen bonding interaction with Leu33 of the MDM2 protein and hydrophobic interactions with Ile40 and Tyr79, while Nutlin-3a showed weaker interactions overall. These results highlight AMJ3 and AMJ5 as promising MDM2 inhibitors with enhanced specificity and efficacy and better activity than Nutlin.

Keywords: MDM2, cancer, protein p53, molecular docking, molecular dynamics

dimethyl sulphoxide

foetal bovine serum

Fourier-transform infrared

Amjad Ibrahim Oraibi: Department of Pharmacy, Al-Manara College for Medical Sciences, Maysan, 62001, Iraq; Department of Pharmaceutical Sciences A, Faculty of Pharmacy of Monastir, University of Monastir, Avicenne Street, Monastir, 5019, Tunisia; Research Laboratory for Bioactive Natural Products and Biotechnology LR24ES14, Faculty of Dental Medicine of Monastir, University of Monastir, Avicenne Street, Monastir, 5000, Tunisia

Ashour H. Dawood: Department of Pharmaceutical Sciences, Al-Esraa University, Baghdad, Iraq

Nawres Debbabi, Leila Chekir-Ghedira: Research Laboratory for Bioactive Natural Products and Biotechnology LR24ES14, Faculty of Dental Medicine of Monastir, University of Monastir, Avicenne Street, Monastir, 5000, Tunisia

Ali Majeed Ali Almukram: School of Pharmacy, University of Maryland, Baltimore, Maryland, United States

Soumaya Kilani-Jaziri: Department of Pharmaceutical Sciences A, Faculty of Pharmacy of Monastir, University of Monastir, Avicenne Street, Monastir, 5019, Tunisia; Research Laboratory for Bioactive Natural Products and Biotechnology LR24ES14, Faculty of Dental Medicine of Monastir, University of Monastir, Avicenne Street, Monastir, 5000, Tunisia

Abbreviations

DMSO

FBS

FTIR

¹ H NMR	proton nuclear magnetic resonance		
MTT	3-(4,5-dimethylthiazol-2-yl)-2,5-diphenyltetra-		
	zolium bromide		
MDM2	murine double minute 2		
RMSD	root mean square deviation		
RMSF	root mean square fluctuation		
MD	molecular dynamics		
MMGBSA	molecular mechanics generalized Born surface area		
MS	mass spectrometry		
PBS	phosphate-buffered saline		
TLC	thin-layer chromatography		

1 Introduction

Cancer remains a significant global health challenge, being one of the leading causes of morbidity and mortality

^{*} Corresponding author: Khalid S. Almaary, Department of Botany and Microbiology, College of Science, King Saud University, P. O. BOX 2455, Riyadh, 11451, Saudi Arabia, e-mail: kalmaary@ksu.edu.sa

^{*} Corresponding author: Fakhreldeen Dabiellil, University of Bahr el Ghazal, Freedowm Street, Wau, 91113, South Sudan, e-mail: researcherzem@gmail.com

worldwide [1]. Despite advances in traditional treatments such as surgery, chemotherapy, and radiation therapy, these approaches are often associated with severe side effects and limited efficacy [2,3]. Thus, there is an urgent need to develop novel therapeutic agents that can selectively and effectively target cancer cells [4]. One promising avenue is targeting the murine double minute 2 (MDM2) protein, a key regulator of the tumour suppressor p53, which plays a central role in cancer therapy. MDM2 binds to p53, leading to its ubiquitination and subsequent degradation via the proteasome system. This regulatory mechanism is critical for maintaining cellular homeostasis [5,6]. Normally, MDM2 binds to p53, triggering its ubiquitination and further degradation through the proteasome system. This control system helps to keep internal balance within the cell [7,8].

In many cancers, MDM2 becomes hyperactive, resulting in excessive degradation of p53 and impairing its tumour-suppressive functions. This allows malignant cells to evade apoptosis, sustain proliferative signalling, and grow uncontrollably. Blocking the MDM2–p53 interaction has thus emerged as an attractive strategy to restore p53 activity and re-enable its anti-tumour potential [9–11]. Existing MDM2 inhibitors, such as Nutlin-3a, have demonstrated promise in preclinical and clinical studies; however, they face significant limitations, including moderate specificity, suboptimal binding affinity, and off-target effects, which can compromise therapeutic outcomes [12–14]. Recent studies have focused on designing inhibitors with enhanced selectivity and efficacy to address these challenges, emphasizing the need for innovative approaches.

Resveratrol, a natural polyphenolic compound found in grapes, berries, and peanuts, is known for its wide range of medicinal properties, including anti-inflammatory, antioxidant, and anti-cancer effects [15,16]. Resveratrol, a natural polyphenolic compound found in grapes, berries, and peanuts, is known for its wide range of medicinal properties, including anti-inflammatory, antioxidant, and anti-cancer effects [17]. However, its low bioavailability and rapid metabolism limit its clinical application, creating an opportunity for structural modifications to enhance its therapeutic potential [18]. To overcome these challenges, we designed and synthesized novel resveratrol-based derivatives to enhance their specificity and efficacy as MDM2 inhibitors. Nevertheless, the practical application of these molecules is hindered due to their low bioavailability and quick metabolism rates. This prompted us to make modifications to resveratrol derivatives to improve therapeutic outcomes.

This study focuses on the design, synthesis, and characterization of four novel resveratrol-based derivatives to address the limitations of existing MDM2 inhibitors. These derivatives incorporate rational structural modifications to retain the beneficial anti-cancer properties of resveratrol while improving

binding affinity, selectivity for cancer cells, and interaction stability with MDM2. The synthesis involved methylation, Vilsmeier-Haack, and conjugation reactions, as detailed in Section 2. The structures and purity of the derivatives were confirmed using mass spectrometry (MS), proton nuclear magnetic resonance (¹H NMR) spectroscopy, and Fourier-transform infrared (FTIR) spectroscopy. We conducted biological evaluations, including MTT assays and MDM2-p53 inhibitory activity, to assess the efficacy of these derivatives. AMJ3 and AMJ5 emerged as the most promising candidates, demonstrating significantly stronger antiproliferative activity against HCT-116 cancer cells and superior selectivity for normal WI-38 cells compared to Nutlin-3a. Computational studies further supported these results, which provided insights into their binding interactions with the MDM2 protein. We conducted molecular docking studies to predict how these resveratrol derivatives would interact with the target protein MDM2 based on its crystal structure (PDB ID: 5ZXF) [19] and evaluate their potential as inhibitors of MDM2. Molecular dynamics (MD) simulations confirmed stable and robust interactions with key residues. Table 1 shows previously published inhibitors [7]. These findings highlight the potential of AMJ3 and AMJ5 as MDM2 inhibitors with enhanced specificity and efficacy, addressing the limitations of current therapies. This study establishes a strong foundation for developing selective MDM2-targeted agents by integrating biological and computational analyses.

2 Experimental section

2.1 General

All reagents and solvents were sourced commercially and utilized without additional purification. The progress of the reactions was tracked using thin-layer chromatography (TLC) on silica gel plates, with visualization achieved under UV light. Column chromatography was conducted employing silica gel with a mesh size of 60–120. The compounds synthesized were analysed through FTIR spectroscopy, MS, and proton nuclear magnetic resonance (¹H NMR) spectroscopy.

2.1.1 General procedure for the synthesis of (*F*)-2,4-dimethoxy-6-(4-methoxystyryl) benzaldehyde derivatives (AMJ1–AMJ6)

Step 1: Synthesis of (E)-1,3-dimethoxy-5-(4-methoxystyryl) benzene (AMJ1)

Resveratrol (1.00 g, 4.38 mmol, 1.0 equiv) was dissolved in 20 mL of DMSO, and 2.95 g (52.5 mmol, 12 equiv) of KOH was added in a single portion at 25°C. DMSO was selected as

Table 1: Identified MDM2 inhibitors that are relevant to clinical study

Compound name	Structure	Mechanism	References
Nutlin-2	Br O N OH	The halogen on the phenyl ring is bromine, enabling the substitution of residues Leu26 and Trp23 on the phenyl ring of p53, with the final residue, Phe19, being replaced by an ethoxy group	[20]
Nutlin-3	Br O NH	Nutlin-3 is a potent small-molecule inhibitor that binds to the MDM2 protein, preventing its interaction with p53. Its structure includes a halogenated phenyl ring, where the bromine atom facilitates interactions with key residues in the MDM2 binding pocket	[21]
Indole-3-carbinol	HO	Phosphorylation at the Ser15 site inhibits the p53-MDM2 interaction	[22]
HDM201	CI N N N O N	Intermittent high-dose pulse treatment with HDM201 induces the expression of PUMA (p53 upregulated modulator of apoptosis) and promotes cell apoptosis in preclinical models, demonstrating <i>in vivo</i> anti-tumour efficacy	[23]
RG7112		Activation of the p53 pathway <i>in vivo</i> triggers apoptosis in tumour cells	[24]
NVP-CGM097	CI N N N N O	Upon binding to MDM2, the structure positions a dihydroisoquinolinone scaffold at the centre of the MDM2 active pocket. This scaffold acts as a connector for three critical moieties, effectively occupying the key active sites of Phe19, Leu26, and Trp23	[25]
APG-115	O OH O OH O N N N N N N N N N N N N N N N N N N N	APG-115 amplifies the anti-tumour efficacy of PD-1 antibodies in Trp53 wild type (Trp53wt), mutant (Trp53mut), and deficient (Trp53) homologous tumour models	[26]
SAR405838 (MI- 77301)	CI H NH NH CI CI	Binding to MDM2 at a pocket analogous to the p53-binding site, Nutlin-3 inhibits the p53-MDM2 interaction, preventing the degradation of p53 and restoring its tumour-suppressing activity	[27]

Table 1: Continued

Compound name	Structure	Mechanism	References
Hoiamide D	MeO OH H N N S S N S N S N S N S N S N S N S	Occupying the hydrophobic binding pocket of MDM2, thereby preventing the interaction between p53 and MDM2	[9]
Idasanutlin (RG7388)	CI FO NH OH	Binding to MDM2 inhibits the formation of the p53/MDM2 complex, thereby stabilizing the p53 protein through post-translational modifications	[28]
AMG 232		Meta-chlorophenyl, para-chlorophenyl, and isopropyl groups of AMG 232 bind to MDM2, preventing its degradation, enhancing stability, and promoting transcriptional activity	[29]
Fluspirilene	O OH O N HN N F	Two fluorophenyl and phenyl groups can fit into either the Leu26 or Phe19 pockets, with the molecule's orientation adjustable to align these groups within the Phe19 and Leu26 pockets	[30]
Isodomoic acid A	HOO O O O O O O O O O O O O O O O O O O	Phosphorylation at the Ser15 residue of p53 inhibits its degradation by MDM2, enhancing both its stability and activity	[31]

the solvent due to its high polarity, which facilitates the dissolution of resveratrol and promotes the methylation reaction by stabilizing the transition state. The reaction was conducted at 25°C to maintain the stability of resveratrol and prevent side reactions at higher temperatures. After stirring the resulting slurry for 5 min at 25°C, 4.99 mL (52.5 mmol, 12 equiv) of dimethyl sulphate was slowly added over 5 min using a syringe. The excess of KOH and dimethyl sulphate (12 equiv each) were used to ensure complete methylation of the hydroxyl groups, maximizing the yield. The reaction mixture was then stirred for 12 h at 25°C.

Workup

Upon completion, the reaction mixture was quenched with 25 mL of saturated aqueous NH4Cl, poured into 10 mL of water, and extracted with 30 mL of EtOAc three times. EtOAc was chosen for its ability to selectively dissolve organic products, facilitating the separation from aqueous impurities. The combined organic extracts were washed with 30 mL of water and 30 mL of brine, dried over MgSO₄, filtered, and concentrated. The resulting crude yellow oil was purified using flash column chromatography (silica gel, hexanes/EtOAc, 8:2) to yield permethylated resveratrol. The hexane/EtOAc ratio was optimized

for the best product separation from byproducts and unreacted starting materials. The yield of the purified product was 84.4%, corresponding to 1 g.

Step 2: Synthesis of (E)-2,4-dimethoxy-6-(4-methoxystyryl)benzaldehyde (AMJ2)

Into a three-necked flask equipped with a stirrer and an immersion thermometer, place 2.6 mL (33.29 mmol) of dry dimethylformamide and immerse the flask in an ice-salt bath. Dry DMF was chosen as the solvent due to its ability to stabilize reactive intermediates and efficiently facilitate the Vilsmeier-Haack reaction. Dimethylformamide was cooled, and gradually, 1 mL (11 mmol) of phosphoryl chloride was added over 30 min. The slow addition of phosphoryl chloride at a controlled temperature prevents exothermic side reactions and ensures the formation of the reactive electrophilic intermediate. Then, over 10 min, a solution of 1 g (3.7 mmol) of permethylated resveratrol was added to 5 mL of anhydrous dimethylformamide, ensuring that the temperature did not exceed 10°C. The mixture was stirred at 10°C for 45 min, then at 35°C for 40 min. Maintaining the temperature below 10°C prevents decomposition of the starting material and unwanted side reactions. When the temperature is increased to 35°C, it promotes the formation of the aldehyde product by completing the reaction.

Workup

After the reaction, as confirmed by TLC, 3 g of crushed ice was added to the mixture and stirred vigorously. Then, 3 g of crushed ice was added. While stirring, slowly add a solution of 2 g of sodium hydroxide to 10 mL of water using a dropping funnel. The addition of sodium hydroxide neutralized the reaction mixture, facilitating the precipitation of the product. The gradual addition prevented excessive foaming and ensured consistent mixing. The solution was added slowly and then increased the speed while maintaining consistent stirring. The product was isolated by filtration, and the 2,4-dimethoxy-6-(4-methoxystyryl)benzaldehyde resulting was washed several times with water. Water washing removed any remaining salts and impurities, ensuring a pure product. The yield of the purified product was 90%, corresponding to 1 g of a yellowish-white powder.

Step 3: Synthesis of (E)-2-(2,4-dimethoxy-6-(4-methoxystyryl)phenyl)-1H-benzo[d]imidazole (AMJ3)

For each reaction, diamine (1 mmol), aldehyde (1.1 mmol), and ammonium acetate (1.5 mmol) were combined in absolute ethanol in a 50 ml round-bottomed flask equipped with a magnetic stirrer. Absolute ethanol was selected as the solvent due to its ability to dissolve all reactants effectively and its role as a benign medium for promoting the formation of the imine intermediate. The flask was loosely capped and heated in an oil bath at 75°C. The reaction temperature of 75°C was optimized to provide sufficient activation energy for the reaction while preventing the decomposition of reactants and products. The progress of the reactions was monitored using TLC with an n-hexane/ethyl acetate (7:1) solvent system. Yield: 66 mg, 19%; mp: $90-92^{\circ}$ C; FT-IR (KBr, ν , cm⁻¹): for 3,460 and 3,414 cm⁻¹, N-H stretching; 3,012 cm⁻¹ aromatic CH stretching, 2,988 cm⁻¹ aliphatic CH stretching for 1,593 cm⁻¹ CC (double bond) alkene; for 1510.74 cm⁻¹, CC (double bond) aromatic, 1,256 cm⁻¹ for C-O stretching, for 1,308 cm⁻¹, NH stretching (secondary amine), for 1,200 cm⁻¹, CN (single bond), ¹H NMR (300 MHz, DMSO-d6) δ 7.81–7.45 (dd, I = 39.1, 8.2 Hz, 2H), 7.45–6.45 (m, 15H), 6.15–5.95 (d, I = 6.2 Hz, 1H), 4.39 - 3.21 (dq, I = 54.8, 40.3 Hz, 24H). Molecular formula: C₂₄H₂₂N₂O₃ molecular weight: 386.45, and mass fragment (m/z): 386.2, 412.

Workup

After the reaction was completed, the solvent was evaporated to obtain the crude product, which was then purified using short-column chromatography with n-hexane/ ethyl acetate (10:1) as the eluent. The n-hexane/ethyl acetate ratio of 10:1 was chosen to achieve effective separation of the desired product from any residual starting materials or byproducts. The yield of the purified product was 19%, equivalent to 66 mg of a yellow powder.

Step 4: Synthesis of (E)-2-amino-4-(2,4-dimethoxy-6-(4-methoxystyryl)phenyl)-4a,10b-dihydro-4H-benzo[h] chromene-3-carbonitrile (AMJ4)

A reaction mixture of 1-naphthol (33 mmol), aldehyde (33 mmol), malononitrile (33 mmol), and piperidine (0.2 ml) in ethanol (15 ml) was heated under reflux for 6 h. Ethanol was chosen as the solvent due to its polar protic nature, which facilitates the solubility of reactants and promotes the nucleophilic addition reaction. Yield: 20 mg, 12%; mp: 138-140°C; FT-IR (KBr, ν , cm⁻¹): for 3,486 and 3,414 cm⁻¹, N-H stretching (symmetric and asymmetric), 3,107 cm⁻¹, for aromatic C-H stretching 2,988 cm⁻¹ for aliphatic CH stretching, 2,208 cm⁻¹, for sharp peak corresponding to the nitrile (cyano) group (C≡N) stretching, 1,593 cm⁻¹ for CC (double bond) alkene, 1,466 cm⁻¹ for CC (double bond) aromatic, 1510.74 cm⁻¹, for CC (double bond) aromatic, 1,256 cm⁻¹, for C-O stretching. 1 H NMR (300 MHz, DMSO-d6) δ 8.66–8.34 (s, 1H), 7.69–7.14 (m, 7H), 7.02-6.92 (d, J = 8.6 Hz, 4H), 6.88-6.74 (d, J = 18.1 Hz, 3H), 6.68-6.57 (m, 1H), 6.56-6.44 (d, J = 16.6 Hz, 1H), 6.06-5.49(d, J = 39.4 Hz, 2H), 4.84–4.53 (s, 2H), 3.98–3.86 (d, J = 8.1 Hz, 5H), 3.81-3.72 (dt, J = 15.4, 7.7 Hz, 10H), 3.02-2.94 (t, J = 5.6 Hz, 1H), 1.68–1.53 (m, 3H)). Molecular formula: C₃₁H₂₆N₂O₄, molecular weight: 490.56, and mass fragment (m/z): 493.8; [M + H].

Workup

After the reaction was completed, the solvent was evaporated to give the crude product, which was purified using short-column chromatography with n-hexane/ethyl acetate (10:1) as eluent. The yield of the purified product was 12%, corresponding to 20 mg of brown powder.

Step 5: Synthesis of (E)-2-amino-4-(2,4-dimethoxy-6-(4-methoxystyryl)phenyl)-4H-chromene-3-carbonitrile (AMI5)

A reaction mixture of 1-naphthol (33 mmol), aldehyde (33 mmol), malononitrile (33 mmol), and piperidine (0.2 ml) in ethanol (15 ml) was heated under reflux for 6 h. Yield: 70 mg, 47%; mp: 132–134 °C; FT-IR (KBr, ν , cm⁻¹): For 3455 and 3,414 cm⁻¹, NH stretching, 3,017 cm⁻¹ for aromatic C–H stretching, 2,988 cm⁻¹ for aliphatic CH stretching, 2,208 cm⁻¹ for CN (triple bond), 1,593 cm⁻¹ for CC (double bond) alkene, 1,510 cm⁻¹ for CC (double bond)aromatic, and 1,153 cm⁻¹ for CO stretching. ¹H NMR (300 MHz, DMSO-d6) δ 7.64–7.51 (m, 1H), 7.42–7.05 (m, 3H), 7.03–6.90 (t, J = 8.7 Hz, 3H), 6.90–6.48 (m, 3H), 4.80–4.66 (s, 0H), 3.96–3.69 (m, 10H), 3.37–3.12 (s, 8H). molecular formula: $C_{27}H_{24}N_2O_4$, molecular weight: 440.50, mass fragment (m/z): 439; [M + H]⁺.

Workup

After the reaction was completed, the solvent was evaporated to give the crude product, which was purified using short-column chromatography with n-hexane/ethyl acetate (10:1) as eluent. The yield of the purified product was 47%, corresponding to 70 mg of brown powder.

Step 6: Synthesis of (E)-2-amino-4-(2,4-dimethoxy-6-(4-methoxystyryl)phenyl)-7-hydroxy-4H-chromene-3-carbonitrile (AMJ6)

A reaction mixture of 1-naphthol (33 mmol), aldehyde (33 mmol), malononitrile (33 mmol), and piperidine (0.2 ml) in ethanol (15 ml) was heated under reflux for 6 h. Yield: 70 mg, 47%; mp: 136–138°C; FT–IR (KBr, ν , cm⁻¹): 3,414 cm⁻¹. broad peak of O–H stretching, 3,304 and 3,291 for NH₂ stretching, 3,100 cm⁻¹ aromatic C–H stretching, 2,934 cm⁻¹ aliphatic C–H stretching, 2,183 cm⁻¹ stretching, for CN, for 1,603 cm⁻¹, C=C stretching (alkene), for 1,491 cm⁻¹, CHCH double bond (aromatic), for 1,238 cm⁻¹, COC stretching. ¹H NMR (300 MHz, DMSO-d6) δ 7.67–7.53 (d, J = 8.6 Hz, 1H), 7.43–7.06 (m, 3H), 7.03–6.41 (m, 7H), 4.16–3.53 (m, 13H), 3.51–3.09 (s, 9H). Molecular formula: $C_{27}H_{24}N_2O_5$, molecular weight: 456.50, and mass fragment (m/z): 472.9; [M–H₂O–H]⁻.

Workup

After the reaction was completed, the solvent was evaporated to give the crude product, which was purified using short-column chromatography with n-hexane/ethylacetate (10:1) as the eluent. The yield of the purified product was 47%, corresponding to 70 mg of brown powder.

3 Biological evaluation

3.1 In vitro MTT cell proliferation assay

3.1.1 Cell culture and media

Human colon carcinoma cells (HCT-116) and normal fibroblast cells (WI-38) were obtained from the Holding Company for

Biological Products and Vaccines (VACSERA, Giza, Egypt). The cells were cultured in RPMI-1640 medium supplemented with 10% foetal bovine serum (FBS) and 1% penicillin–streptomycin solution (100 IU/mL penicillin and 0.1 mg/mL streptomycin). All cultures were maintained at 37°C in a humidified incubator with 5% CO₂.

3.2 Procedure

The MTT assay was conducted to evaluate the antiproliferative activity of the synthesized compounds. MTT (3-[4,5-dimethylthiazol-2-yl]-2, 5-diphenyltetrazolium bromide; Sigma) was dissolved in phosphate-buffered saline (PBS) at a concentration of 5 mg/mL. The solution was filtered to remove any insoluble residue and sterilized. For the assay, 2.6×10^4 to 3×10^4 cells were seeded into each well of a 96-well tissue culture plate and incubated for 24 h to allow adherence. Drug stock solutions were prepared in dimethyl sulphoxide (DMSO) and serially diluted in a culture medium to achieve eight concentrations (300, 100, 30, 10, 3, 1, 0.3, and $0.1 \mu g/mL$). Cells were treated with these solutions for 72 h, while untreated cells were the control group. After treatment, 10 µL of freshly prepared MTT solution was added to each well, resulting in a final concentration of $0.5 \,\mu\text{g/}\mu\text{L}$. The plates were incubated for 4 h at 37°C, during which viable cells reduced MTT to insoluble purple formazan crystals. To dissolve the crystals, 200 µL of a 1:1 mixture of DMSO and isopropanol was added to each well, and the plates were incubated for 30-45 min at room temperature. Absorbance was measured at 590 nm using a Multiskan® EX Microplate Reader (Thermo Scientific, USA). The assay was performed three times, with each experiment conducted in triplicate. The IC₅₀ values, defined as the concentration required to inhibit 50% of cell proliferation, were determined using nonlinear regression analysis in GraphPad Prism 8 software.

3.3 Evaluation of MDM2 inhibition activity

3.3.1 Biological assessment of the p53/MDM2 complex – specific enzyme immunoassay

The potential of the synthesized compounds to inhibit the interaction between the p53 tumour suppressor protein and MDM2 protein was evaluated using a p53/MDM2 enzyme-linked immunosorbent assay (ELISA). Capture antibodies (100 μ L; prepared at 250× in coating buffer)

were dispensed into the wells of a 96-well plate, sealed, and incubated overnight at room temperature. The next day, the coating solution was aspirated, and 200 µL of blocking buffer was added to each well to prevent nonspecific binding. The plates were incubated for 1h at room temperature and then aspirated to remove the blocking solution. p53 standards, prepared in 20× stock analysis buffer at a concentration of 1 µg/mL, were pipetted into the bottom of the appropriate wells. MDM2 standards, prepared in 20× stock analysis buffer at a concentration of 0.32 µg/mL, were added to polypropylene-capped microvials. Test compounds and Nutlin-3 (a reference MDM2 inhibitor), dissolved in DMSO at a concentration of 20 µM, were added to the microvials. The mixtures were pipetted up and down for thorough mixing and incubated for 1h at room temperature in a WiseCube incubator (witeg Labortechnik GmbH, Wertheim, Germany).

Following incubation, 50 µL of each MDM2 mixture was transferred to the corresponding wells containing p53, and the plates were incubated on a plate shaker for 1h at room temperature. Wells were then washed four times with 400 µL of wash solution. A diluted MDM2 detection antibody (250× stock in assay solution) was added to each well, except for the blank, and the plate was incubated for another hour on a shaker at room temperature. After washing the wells four times, 100 µL of streptavidinhorseradish peroxidase complex was added to each well (excluding the blank), and the plates were incubated for 30 min. The wells were washed again, and 100 µL of tetramethylbenzidine substrate was added to each well. The reaction was allowed for 30 min at room temperature, after which 100 µL of 1 N hydrochloric acid was added to stop the reaction. Absorbance was measured at 450 nm using a MultiSkan™ GO Microplate Spectrometer (Thermo Fisher Scientific, Waltham, MA, USA). Eight concentrations of each compound (30, 10, 3, 1, 0.3, 0.1, 0.03, and 0.01 µM) were tested, and all results are expressed as the mean ± standard deviation from three determinations performed in replicates (n = 6). The IC50 values were calculated from sigmoidal dose-response curves using GraphPad Prism 8 software.

3.4 Computational studies

3.4.1 Molecular docking studies

Molecular docking analysis explored the interaction between the synthesized compounds and the MDM2 protein using the Glide module in Maestro software [32]. The 3D structure of the protein (PDB ID: 5ZXF) [19] was obtained from the Protein Data Bank (PDB). The protein for docking was prepared through the Protein Preparation Wizard, which filled in missing residues and refined overall structural integrity. Ligands were prepared with the OPLS3 force field at a pH of 7.0 \pm 2 [33]. To improve the accuracy of binding affinity predictions, we used the Xp Glide algorithm (OPLS3 force field) available in Maestro, which is a reliable method for prediction.

3.4.2 MD simulation

Using the Desmond software package (Schrödinger LLC), MD simulations were conducted for 150 ns. Molecular docking was performed before the MD simulation to obtain the molecule's static binding location on the protein's active site. We performed MD simulations to study the ligand-binding status in the physiological environment, allowing atoms to move according to Newton's classical equation of motion over time [34]. The ligand-protein complex was generated by Maestro's Protein Preparation Wizard, which optimized, minimized, and filled missing residues [35]. The system was created by System Builder. The system was solvated with an orthorhombic box and TIP3P (Intermolecular Interaction Potential 3 Points Transferable) solvent model, at 300 K/1 atm and using the OPLS 2005 force field. Neutralization with counter ions and 0.15 M sodium chloride was performed to imitate physiological conditions in the models [36,37]. The models were equilibrated before the simulation and recorded trajectories every 150 ps for analysis.

4 Results and discussion

4.1 Chemistry

The synthesis of the derivatives (AMJ1-AMJ6) involved a series of carefully orchestrated chemical transformations, beginning with the permethylation of resveratrol to obtain (E)-1,3-dimethoxy-5-(4-methoxystyryl) benzene (AMJ1), followed by a Vilsmeier-Haack formylation to obtain (E)-2,4dimethoxy-6-(4-methoxystyryl)benzaldehyde (AMJ2), and subsequent steps to build the target molecules with benzodiazole and chromene cores (Scheme 1). The conversion of resveratrol to AMJ1 was performed under mild conditions using DMSO and KOH, followed by methylation with dimethyl sulphate. The reaction proceeded smoothly, and the product was isolated with an 84.4% yield after flash

chromatography, demonstrating the efficiency of the permethylation step. The method was robust, producing the desired product with minimal side reactions. The formylation of AMJ1 was successfully carried out using DMF and POCl₃ under controlled low-temperature conditions. AMJ2 was synthesized with good selectivity, yielding 90% after aqueous workup and crystallization, underscoring the effectiveness of the Vilsmeier–Haack reaction for generating substituted benzaldehydes. Subsequently, AMJ3 was condensed with various amines and reagents to produce benzodiazole and chromene derivatives. The FTIR

spectrum of AMJ3 displayed two significant peaks at 2,988 cm⁻¹ (C–H stretching vibrations) and 1,593 cm⁻¹ (aromatic C=C stretching), indicating the presence of a benzene derivative (Figure S1). MS revealed a molecular ion peak at m/z 312 [M+], aligning with the calculated molecular weight (Figure S5). The ¹H NMR spectrum of AMJ3 in DMSO-d6 showed signals at δ 7.45–6.95 ppm (aromatic protons) and δ 3.80 ppm (methoxy groups), confirming the substitution pattern on the benzene ring (Figure S6) (Scheme 1). The FTIR spectrum of AMJ4 showed a strong peak at 1,593 cm⁻¹, characteristic of the aldehyde C=O

Scheme 1: Synthesis of the target compounds AMJ1–AMJ6 under the synthesis condition. Synthesis of the target compounds (AMJA–AMJ6). (i: heat 25®C, 12 h, DMSO, KOH, dimethyl sulfate; ii: POCl3, NaOH, reflux, anhydrous dimethylformamide, 10–15®C, 0.45 h; iii: diamine (1mmol), aldehyde (1.1 mmol), ammonium acetate (1.5 mmol), reflux, heat, 75®C, 2 h; iv: 1-naphthol (33 mmol), aldehyde (33 mmol), malononotrile (33 mmol) and piperidine (0.2 ml) in ethanol (15 ml), reflux 6 h, heat, 25®C; v: 1-naphthol (33 mmol), aldehyde (33 mmol), malononotrile (33 mmol) and piperidine (0.2 ml) in ethanol (15 ml), reflux 6 h, heat, 25®C.

stretch, along with typical aromatic C=C stretches around 1,600 cm⁻¹. The MS spectrum revealed a molecular ion peak at m/z 326 [M+], in agreement with its molecular formula. Distinctive aldehyde proton signal appeared in its ¹H NMR spectrum at δ 9.84 ppm, while other aromatic protons resonated between δ 7.60 and δ 6.90 ppm (Figure S2). Notably, compound AMJ3 had a moderate yield (19%) when it was synthesized by the condensation reaction of diamine. The low yield could be attributed to the formation of regioisomers or incomplete reaction under the set conditions. Improvements in yield might be explored through optimization of the reaction time and temperature. AMI4 showed an FTIR spectrum with peaks at 3,468 and 3,414 cm⁻¹ for N-H stretching, 3,012 cm⁻¹ for aromatic CH stretching, 2,988 cm⁻¹ for aliphatic CH stretching and 1,593 cm⁻¹ for CC (double bond) alkene, 1510.74 cm⁻¹ for CC (double bond) aromatic, 1,308 cm⁻¹ for NH stretching (secondary amine), 1,200 cm⁻¹ for CN (single bond), and 1.153 cm⁻¹ for CO (single bond), an NH stretching band at 3,305 cm⁻¹ and a C=O stretch at 1,655 cm⁻¹, typical for benzodiazoles. Its mass spectrum presented a base peak at m/z 386.2, fitting the molecular weight. The ¹H NMR data included aromatic proton signals at δ 7.81–7.45 ppm and δ 7.45–6.45 ppm, with additional peaks due to the NH group at δ 8.10 ppm (Figure S6).

AMJ5 and AMJ6 were synthesized via a Knoevenagel condensation followed by a cyclization to form chromene derivatives. The yields varied, with AMJ4 at 12% and AMJ5 at a significantly higher 47%, indicating a possible influence of reaction kinetics and thermodynamic stability on the final product formation. AMJ5 and AMJ6, both chromene derivatives, exhibited similar spectral features with key differences. The FTIR spectrum of AMJ5 had notable peaks for NH and CN stretching at 3,455 and 2,208 cm⁻¹ respectively (Figures S3 and S4). Its ¹H NMR spectrum showed aromatic protons at δ 7.69–6.57 ppm and a nitrile group signal at δ 8.66 ppm. AMJ6 differed slightly, with its FTIR spectrum showing NH stretching at 3,414 cm⁻¹ and CN stretching at 2,208 cm⁻¹. The ¹H NMR spectrum included aromatic protons at δ 7.64–6.48 ppm and lacked the nitrile group's high-field signal. The high yield in the synthesis of AMJ6 suggests an efficient cyclization step under the reflux conditions provided. AMJ6, incorporating a hydroxy group, was also synthesized in a 47% yield, like AMJ5, which suggests that the introduction of a hydroxy group at the 7position on the chromene ring does not significantly hinder the reaction process. AMJ6's spectral data were indicative of a hydroxy-substituted chromene. The FTIR spectrum had a broad O-H stretch at 3,414 cm⁻¹ of compound AMJ5, along with other functional group absorptions. The MS and ¹H NMR spectra were similar to AMJ6 but included shifts in the aromatic region, suggesting the influence of

the hydroxy group on the electronic environment of the aromatic system. Characteristic absorption bands in the FTIR spectra and the correct mass peaks in MS ensured the structural integrity of the compounds. The ¹H NMR spectra provided conclusive evidence for the structures of AMJ1-AMJ6, with chemical shifts corresponding to the expected molecular environments. The synthesized series of derivatives AMJ1-AMJ6 highlighted the versatility of benzaldehyde derivatives as precursors for the synthesis of complex molecules like benzodiazoles and chromenes. The varying yields across the synthesis steps underscore the need for further optimization to enhance reaction efficiency and product recovery. The successful characterization of these compounds will pave the way for their potential evaluation in biological studies in future studies.

4.2 In vitro MTT cell proliferation assay

The MTT assay evaluated cell viability in response to treatment with different compounds. The results, summarized in Table 2, indicate the percentage of antiproliferative activity against human colon cancer cells (HCT-116) (Figure 1) and their effects on normal lung fibroblast cells (WI-38) to assess the selectivity and safety of the compounds (Figure 2). All cells were treated for 72 h.

HCT-116 cells treated with varying concentrations of the compounds (0.1, 100, and 300 µg/mL) for 72 h were also observed under an inverted microscope to assess morphological changes (Figures 3-5).

4.3 MTT assay results

The IC₅₀ values of the tested compounds against the HCT-116 cell line were determined using the MTT assay. The results are presented as mean ± standard deviation (SD) from three independent experiments performed in triplicate. Statistical analysis was conducted using one-way

Table 2: Antiproliferative activity of compounds on HCT-116 and WI-38

Compound	Sample	In vitro cytotoxicity [IC ₅₀ , μg/mL ± SD]	
		HCT-116	WI-38
1	AMJ3	22.69 ± 2.47	75.86 ± 2.73
2	AMJ4	44.50 ± 1.77	86.70 ± 3.75
3	AMJ5	23.18 ± 2.55	67.25 ± 4.50
4	AMJ6	84.39 ± 2.99	97.94 ± 3.07
Nutlin-3a		62.72 ± 3.15	124.90 ± 3.06

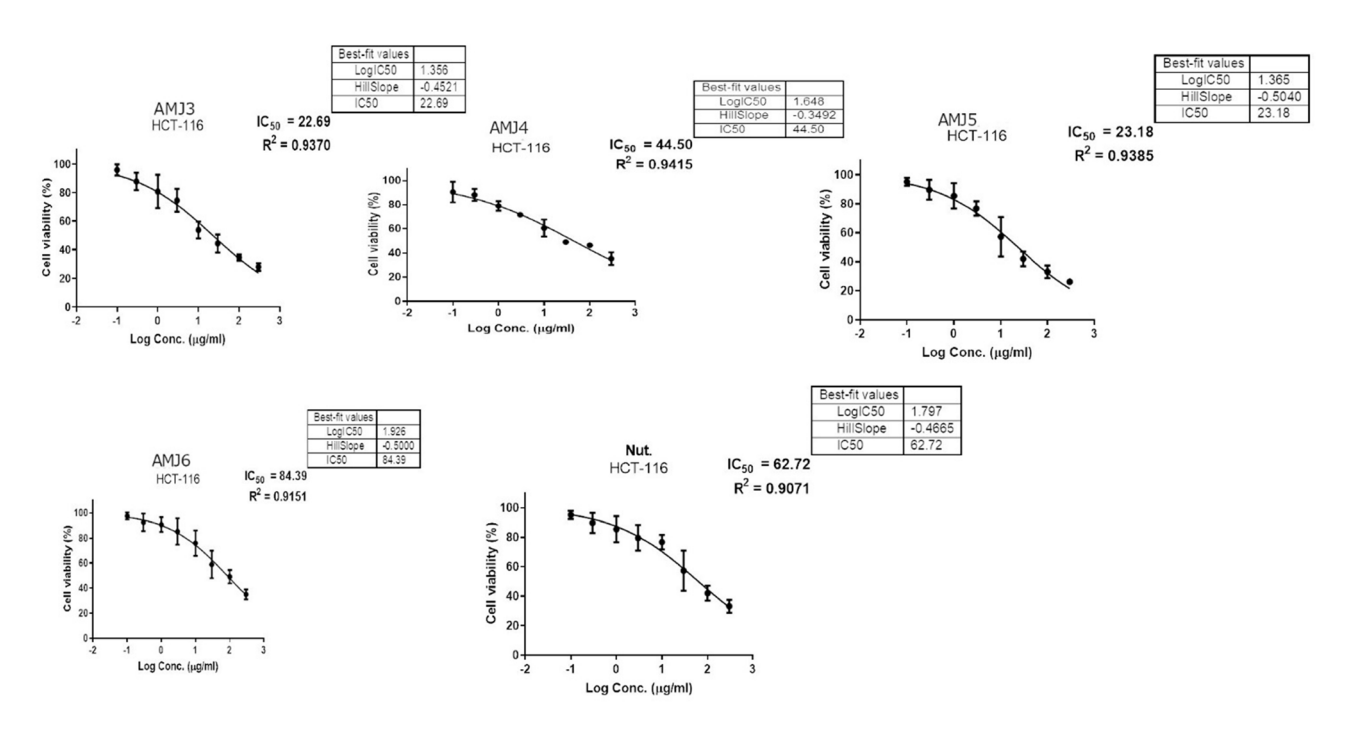


Figure 1: Antiproliferative activity with IC₅₀ values of compounds and nutlin reference against HCT-116 cells.

ANOVA, followed by Tukey's post-hoc test to assess significant differences among the tested compounds. The significance level was set at p < 0.05, as shown in Figures 6 and 7.

Among the tested compounds, compound 3 (AMJ3) exhibited the strongest antiproliferative activity against

HCT-116 cells with an IC₅₀ value of 22.69 \pm 2.47 µg/mL, outperforming that of the reference compound Nutlin (IC₅₀: 62.72 \pm 3.15 µg/mL). Compound 3 (AMJ3) also displayed high selectivity towards normal WI-38 cells, with an IC50 value of 75.86 \pm 2.73 µg/mL. These results suggest that compound

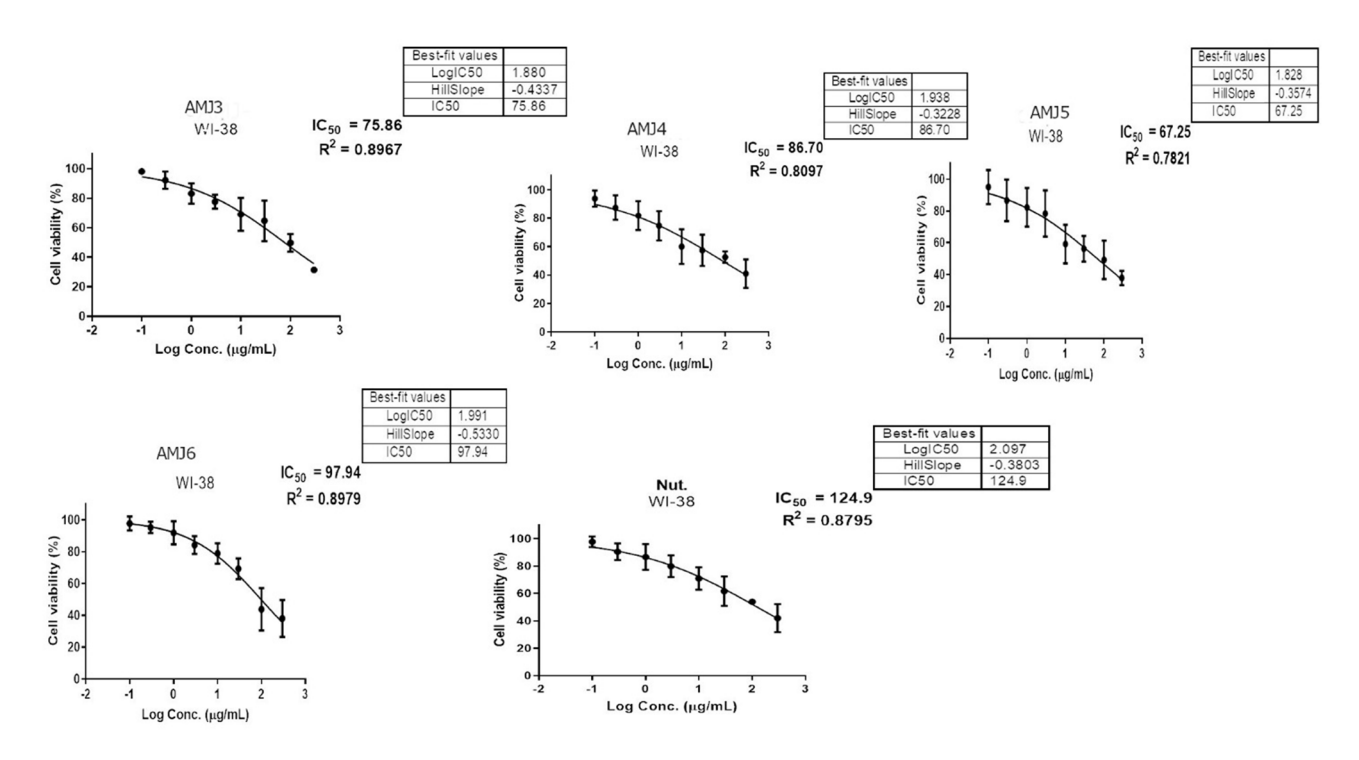


Figure 2: Antiproliferative activity with IC₅₀ values of compounds and nutlin reference against WI-38 normal lung fibroblast cells.

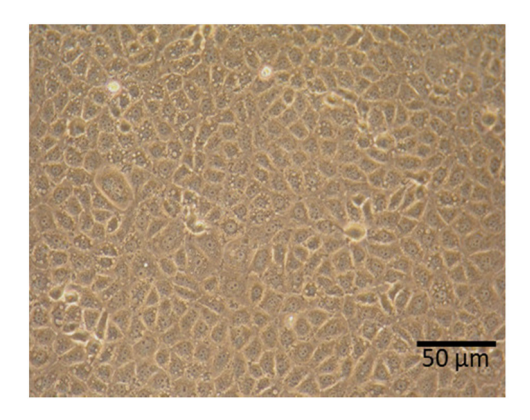


Figure 3: Image of the control CHT-116 cells.

3 (AMJ3) is a promising anticancer agent, capable of selectively targeting cancer cells while sparing normal cells. Compound 5 (AMJ5) also demonstrated strong antiproliferative activity, with an IC $_{50}$ of 23.18 \pm 2.55 µg/mL, comparable to compound 3 (AMJ3). It exhibited good selectivity toward normal cells (IC $_{50}$: 67.25 \pm 4.50 µg/mL), further supporting its potential as an anticancer candidate. Compound 4 (AMJ4) showed moderate activity against HCT-116 cells, with an IC $_{50}$ of 44.50 \pm 1.77 µg/mL, making it less potent than compound 3 (AMJ3) and compound 5 (AMJ5). Furthermore, its selectivity towards normal cells (IC $_{50}$: 86.70 \pm 3.75 µg/mL) was lower, limiting its potential as a selective anticancer agent. Compound 6 (AMJ6) exhibited the weakest antiproliferative

activity, with an IC $_{50}$ value of 84.39 ± 2.99 µg/mL and poor selectivity towards normal cells (IC $_{50}$: 97.94 ± 3.07 µg/mL), making it the least effective compound compared to the reference Nutlin.

4.3.1 MDM2 inhibitory activity results

The MDM2 inhibitory activity of the compounds was evaluated using a p53-MDM2 ELISA assay, and the results are summarized in Table 3.

4.3.2 MDM2 inhibition

Compound 3 (AMJ3) exhibited the strongest inhibitory activity against the MDM2–p53 interaction, with an IC $_{50}$ value of 0.24 \pm 0.02 μ M, surpassing the reference Nutlin-3a compound (IC $_{50}$: 0.39 \pm 0.03 μ M). This potent inhibitory activity suggests a strong binding affinity of AMJ3 to the MDM2–p53 complex, effectively disrupting the interaction and restoring p53 function. When combined with its potent antiproliferative activity against HCT-116 and selectivity toward WI-38 cells, AMJ3 emerges as a highly promising anticancer candidate. Compound 5 (AMJ5) also demonstrated significant inhibitory activity, with an IC $_{50}$ value of 0.48 \pm 0.04 μ M, comparable to Nutlin-3a. Along with its strong results in the MTT assay, compound 5 (AMJ5) shows

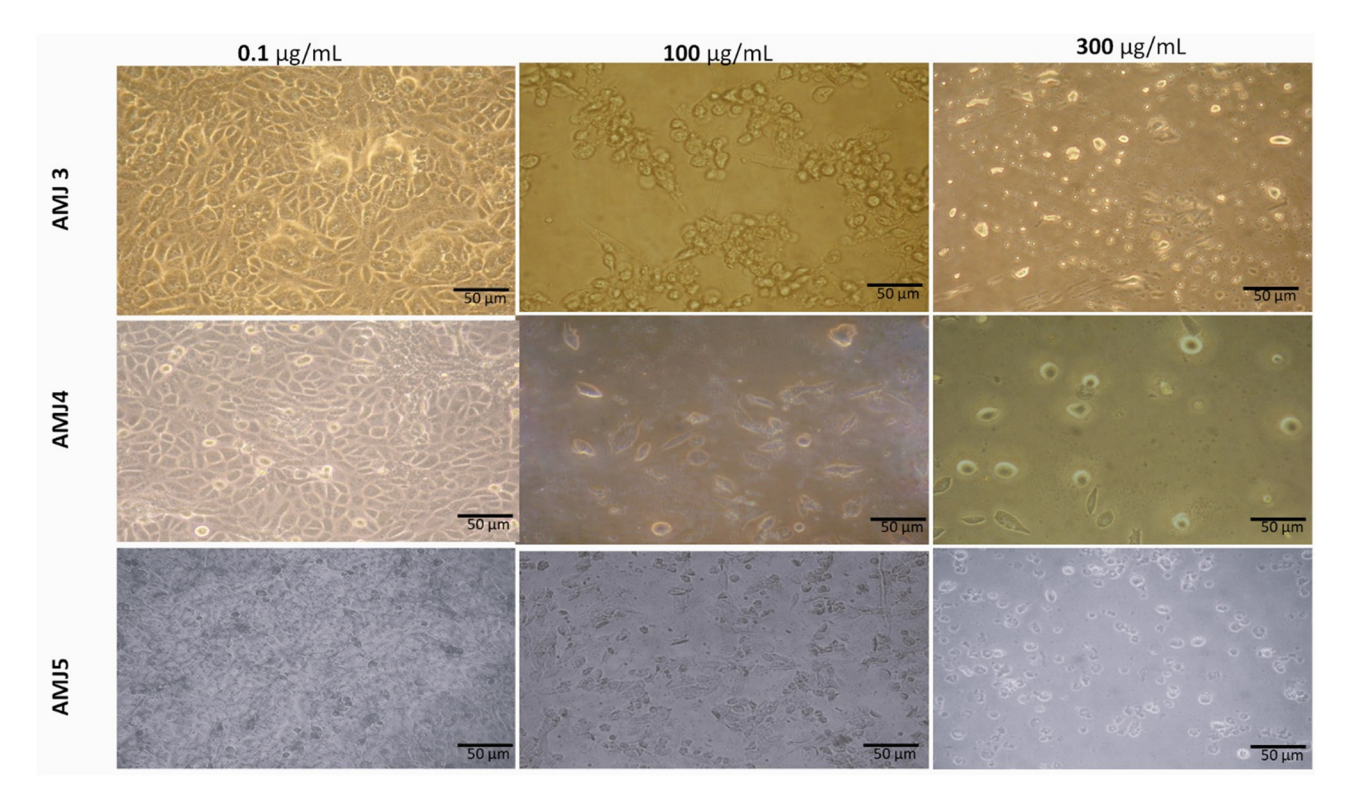


Figure 4: Effects of AMJ3, AMJ4, and AMJ 5 on the HCT-116 cell line at concentrations of 0.1, 100, and 300 for 72 h.

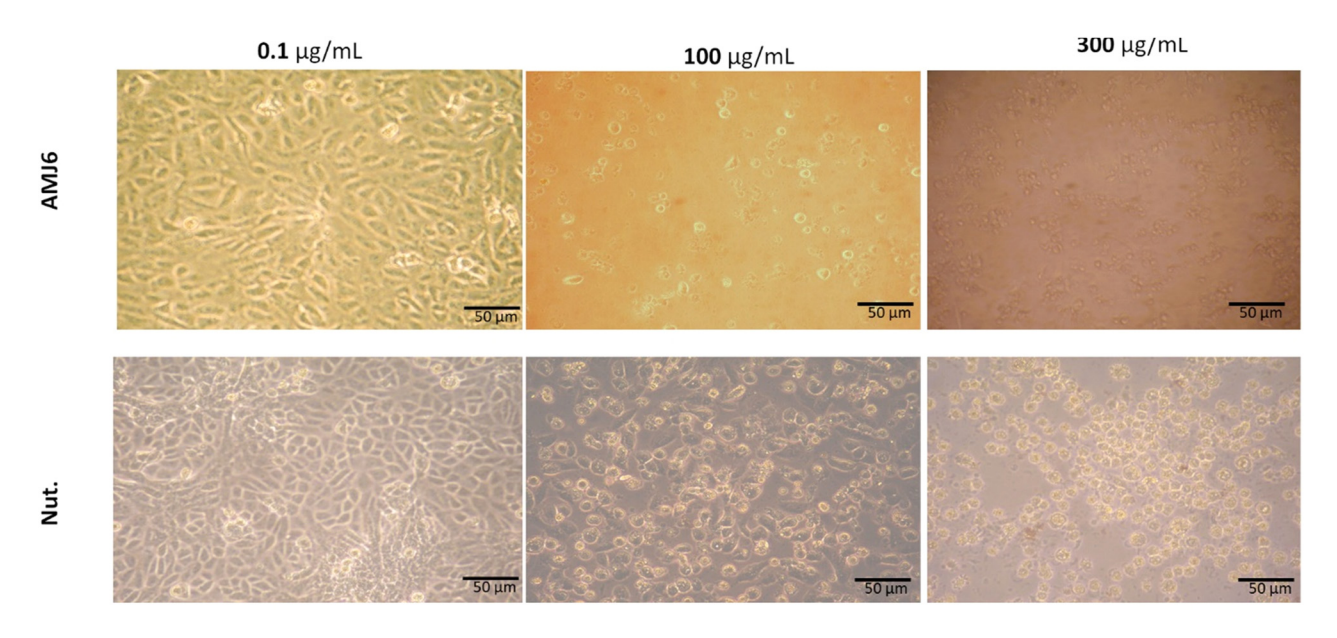


Figure 5: Effect of AMJ6 and reference Nutlin on the HCT-116 cell line at concentrations of 0.1, 100, and 300 µg for 72 h.

potential as another viable anticancer candidate. In contrast, Compound 4 (AMJ4) exhibited weaker MDM2 inhibition, with an IC $_{50}$ value of 2.55 \pm 0.40 μ M, making it less effective than Nutlin-3a. Similarly, compound 6 (AMJ6) displayed poor MDM2 inhibitory activity (IC $_{50}$: 2.63 \pm 0.46 μ M), indicating limited potential as an anticancer agent.

4.4 Molecular docking

Molecular docking studies assessed the interaction between synthesized compounds (AMJ3, AMJ4, AMJ5,

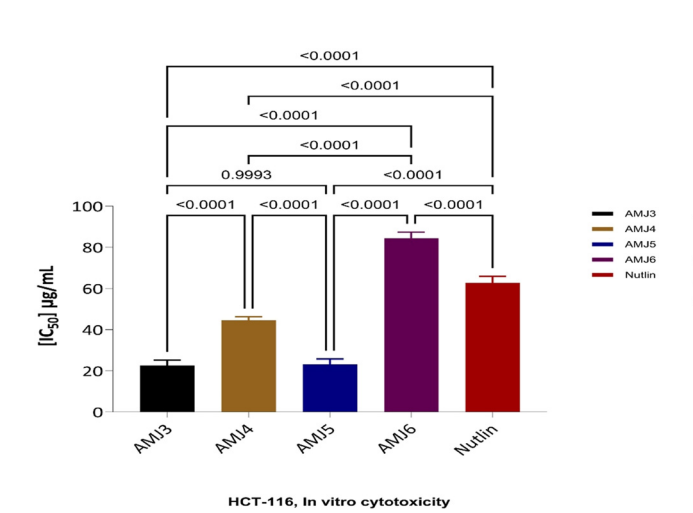


Figure 6: IC_{50} values of the tested compounds against HCT-116 cells (mean \pm SD). Statistical analysis was performed using one-way ANOVA followed by Tukey's test (p < 0.05).

AMJ6) and the MDM2 protein, a pivotal target in cancer therapy. The computational analysis revealed distinct binding affinities and modes of interaction. Nutlin-3a, serving as a benchmark with a binding affinity of -6.903 and MMGBSA with a binding energy ΔG of -19.09 kcal/mol, showed extensive interactions predominantly via hydrogen bonds with Gln51 along with significant hydrophobic contacts throughout the binding site (Figure 8). In the molecular docking studies, AMJ4 and AMJ5 demonstrated lower binding affinities to the MDM2 protein,

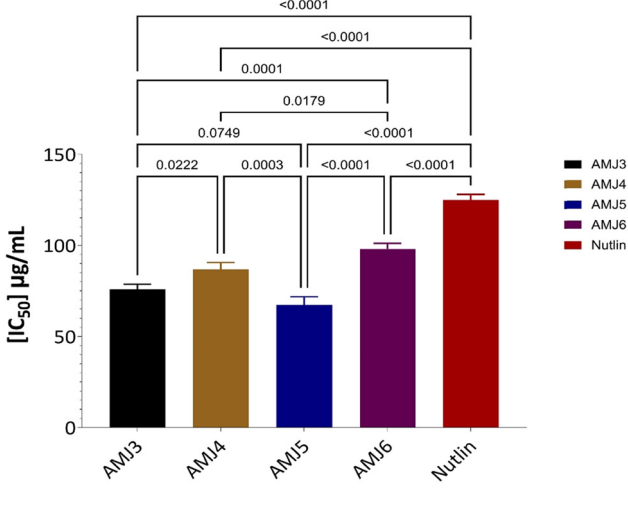


Figure 7: IC_{50} values of the tested compounds against WI-38 cells (mean \pm SD). Statistical analysis was performed using one-way ANOVA followed by Tukey's test (p < 0.05).

WI-38, In vitro cytotoxicity

Table 3: Inhibitory activity of compounds against MDM2–p53 interaction

Compound	Code	Mdm2-p53 inhibition [IC ₅₀ , μ M \pm SD]
1	AMJ3	0.24 ± 0.02
2	AMJ4	2.55 ± 0.40
3	AMJ5	0.48 ± 0.04
4	AMJ6	2.63 ± 0.46
Nutlin-3a		0.39 ± 0.03

with glide scores of -4.3 and -3.9, respectively, compared to AMJ3 and AMJ6, which showed glide scores of -5.6 and -4.9, respectively. These results suggest that AMJ4 and AMI5 may have weaker interactions with MDM2, potentially resulting in less effective inhibition. AMJ3 and AMJ6 displayed notably higher binding energies, -35.53 and -39.39 kcal/mol, respectively, suggesting a stronger and potentially more stable interaction with MDM2. These compounds formed key hydrogen bond linkages with residues such as His75 with AMJ3 compound and Gln51 with AMJ6, and other hydrophobic interactions were observed as hydrophobic interactions such as Leu33, Phe34, and Phe65 (Figure 8). An in-depth analysis of ligands revealed that the presence of additional functional groups, such as nitrogen and oxygen, in AMJ compounds allowed for more diverse interactions. The benzene ring linked to nitrogen

in AMJ3 participated in π - π stacking with His75 and Tyr79 with the oxygen atom of the benzene ring, which may potentially enhance molecular binding stability.

Similarly, the amino group present within the fused ring system of AMJ6 formed hydrogen bonds and hydrophobic contacts, respectively, with polar side chains of Gln51 and His52, thus enhancing binding specificity and strength. Their remarkable binding energies compared to Nutlin-3a indicate that AMJ3 and AMJ6 could be better MDM2 inhibitors. The surface view of the 3D image indicated favourable binding affinity in the MDM2 protein (Figure 9). Further examination revealed that the main contact between AMJ4s and MDM2 protein is hydrophobic interaction. Specifically, a benzene ring forms a hydrophobic contact with His52, an essential residue located at the binding pocket of MDM2.

On the other hand, AMJ5's interaction with MDM2 involves a hydrogen bond, but it is with a water molecule rather than directly with an amino acid residue of the protein (Figure 10). While molecular docking provides valuable insights into potential binding poses and affinities, it is based on static structures, which may not fully represent the dynamic conformational changes that occur during ligand binding. Moreover, the docking process simplifies the binding environment by excluding solvent effects and entropy changes, which can influence the true binding affinity in biological systems.

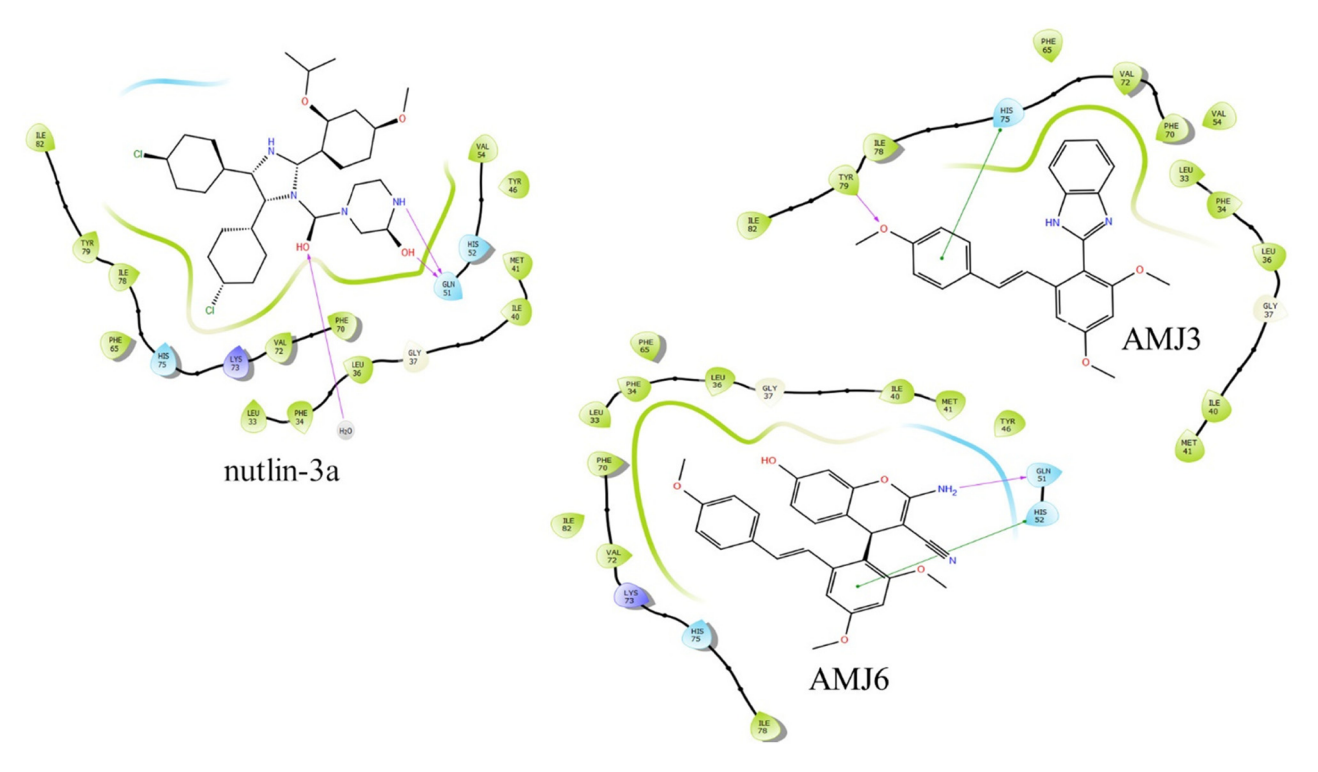


Figure 8: 2D interaction of the protein and ligand complex of compounds AMJ3, AMJ6, and co-crystal ligand Nutlin-3a.

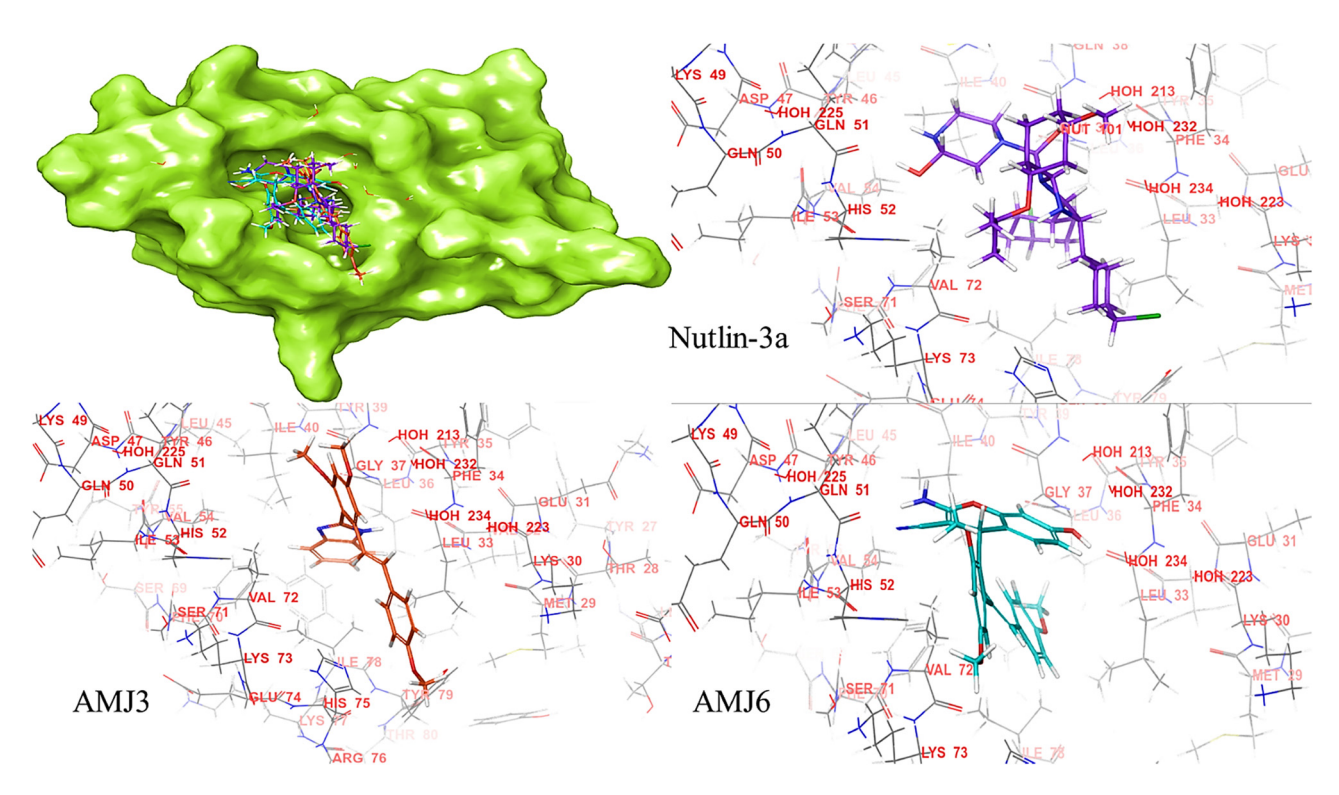


Figure 9: Surface view of the protein and ligand contact and 3D interaction of the protein and ligand complex of compounds AMJ3, AMJ6, and co-crystal ligand nutlin-3a.

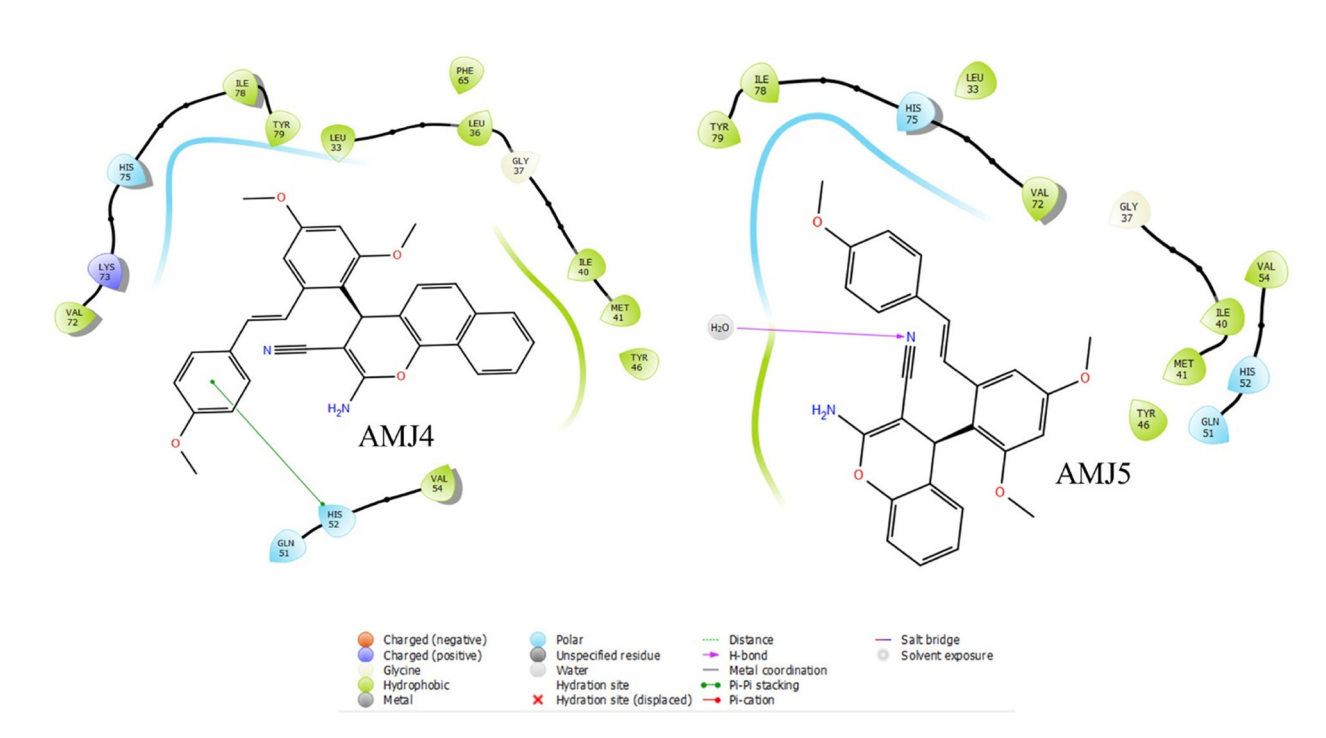


Figure 10: 2D interaction of the protein and ligand complex of compounds AMJ4 and AMJ5.

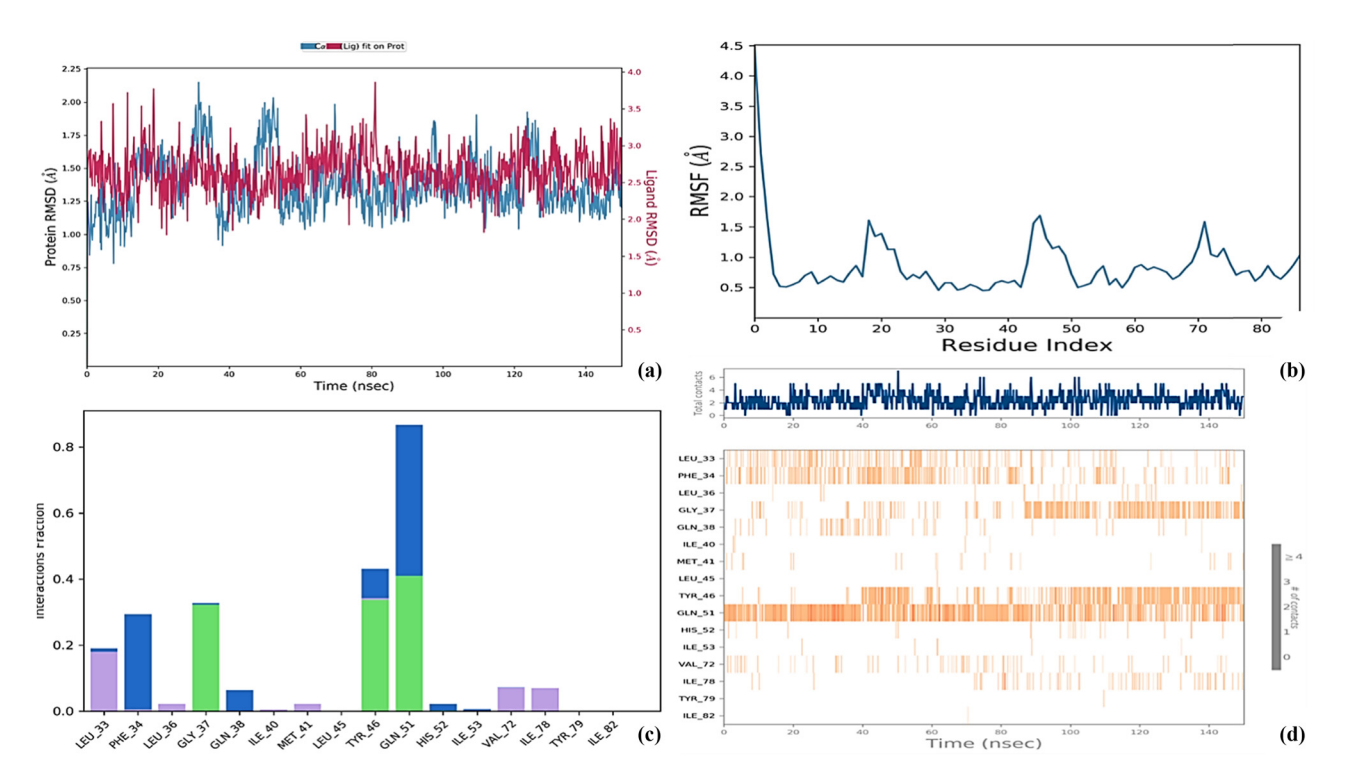


Figure 11: Molecular dynamics simulation analysis of the co-crystal ligand Nitulin-3a: Image (a) shows the RMSD of the protein and ligand complex; Image (b) shows the RMSF of the protein; Image (c) shows the protein and ligand contact histogram (green colour shows the H-bonding interaction, blue colour shows water bridges, and pink colour shows hydrophobic interaction), and Image (d) shows the protein and ligand contact in heatmaps analysis.

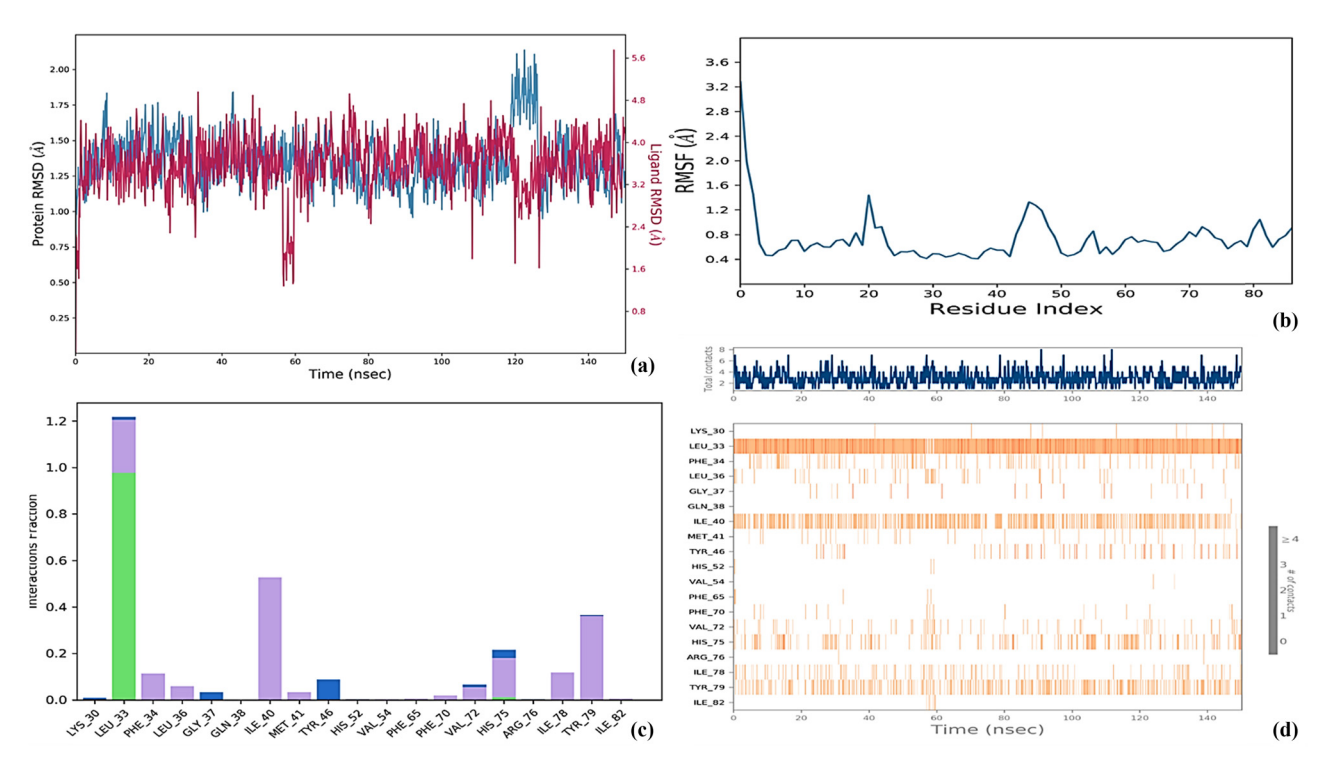


Figure 12: Molecular dynamics simulation analysis of compound AMJ3: Image (a) shows the RMSD of the protein and ligand complex; Image (b) shows the RMSF of the protein; Image (c) shows the protein and ligand contact histogram (green colour shows the H-bonding interaction, blue colour shows water bridges, and pink colour shows the hydrophobic interaction), and Image (d) shows the protein and ligand contact in heatmaps analysis.

4.5 MD

A detailed MD simulation was conducted for 150 ns using Desmond software to investigate the formation of stable complexes involving compounds AMJ3, AMJ6, the co-crystal ligand nutlin-3a, and the target protein MDM2 (Figures 11–13). The study focused on critical parameters, including root mean square deviation (RMSD), root mean square fluctuation (RMSF), and protein–ligand interactions.

4.5.1 RMSD analysis

The RMSD values of the C-alpha atoms in the protein complexes provided insights into the overall stability of the ligands within the binding pocket. Compound AMJ3 exhibited stable RMSD values, maintaining an average of 1.30 Å after 20 ns. Notably, transient fluctuations were observed between 55–60 and 118–126 ns, where RMSD values briefly dropped to 1.27 Å before stabilizing again at 1.30 Å (Figure 12). These fluctuations did not compromise the overall stability of the AMJ3–MDM2 complex, which remained comparable to the Nutlin-3a ligand. In contrast, AMJ6 displayed an initial equilibration phase lasting approximately 45 ns,

with RMSD values fluctuating around 1.45 Å during this period. After equilibration, AMJ6 maintained a consistent RMSD of approximately 1.50 Å, reflecting stable binding within the MDM2 pocket throughout the simulation (Figure 13). These findings suggest that AMJ6 achieves a high level of stability after the initial phase, making it a strong candidate for MDM2 inhibition.

4.5.2 RMSF analysis

The RMSF analysis revealed the extent of flexibility in specific regions of the protein–ligand complex. Both AMJ3 and AMJ6, as well as the Nutlin-3a ligand, displayed lower fluctuations at the binding site, particularly in the loop and terminal regions of the protein. This reduction in RMSF values underscores the stability and durability of interactions between the protein and ligands. Furthermore, preserving secondary structural elements, including alphahelices and beta-strands, accounted for 47.09% of the overall protein structure, ensuring structural integrity throughout the simulation. Alpha-helices and beta-strands contributed 38.79 and 7.30%, respectively, to the protein's secondary structure in the presence of Nutlin-3a.

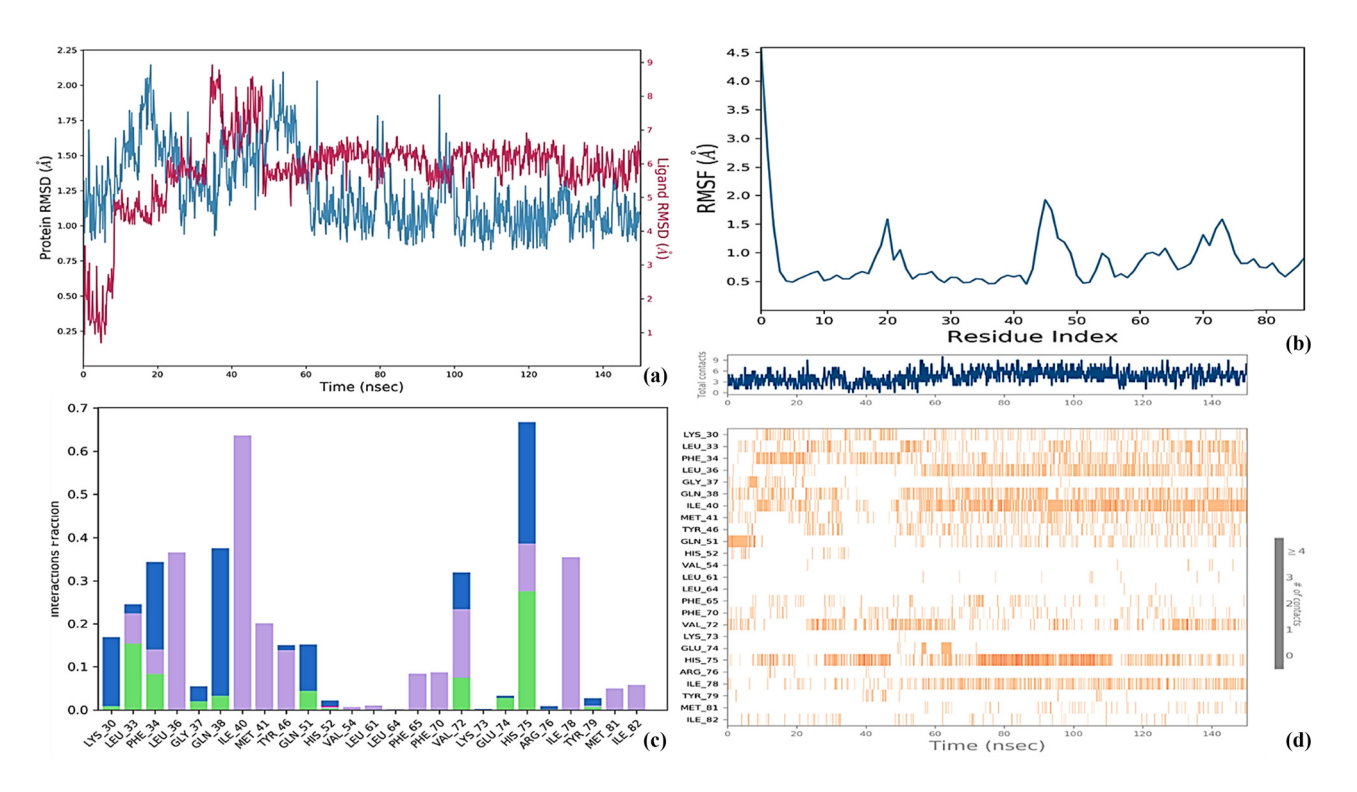


Figure 13: Molecular dynamics simulation analysis of compound AMJ6: Image (a) shows the RMSD of the protein and ligand complex; Image (b) shows the RMSF of the protein; Image (c) shows the protein and ligand contact histogram (green colour shows the H-bonding interaction, blue colour shows water bridges, and pink colour shows the hydrophobic interaction), and Image (d) shows the protein and ligand contact in heatmaps analysis.

4.5.3 Protein-ligand interaction analysis

Detailed interaction analysis revealed the specific residues involved in binding for each ligand. Compound AMJ3 demonstrated a strong hydrogen bonding interaction with Leu33 of the MDM2 protein, with a 97% interaction fraction. Additional hydrophobic interactions were observed with Ile40 and Tyr79, further stabilizing the complex. Similarly, AMJ6 exhibited hydrophobic interactions with Ile40, Ile78, and Leu36 and an additional hydrogen bond with His75 of the protein (Figure 13). In contrast, Nutlin-3a formed hydrogen bonds with Gly37 and Gln51 via its piperazine moiety, contributing to only 33% of the protein's interactions (Figure 11). These findings highlight the enhanced binding affinity and stability of AMJ3 and AMJ6 compared to Nutlin-3a, suggesting their potential as superior MDM2 inhibitors.

5 Limitations of the study

While this study highlights the potential of novel resveratrol-based derivatives as MDM2 inhibitors, some limitations should be acknowledged. Although computational findings were supported by in vitro experiments, such as MTT assays and MDM2-p53 inhibition studies, the absence of in vivo validation limits the ability to fully assess the pharmacokinetics, toxicity, and therapeutic efficacy of the compounds in more complex biological systems. Future studies incorporating animal models will be essential to bridge this gap and confirm the translational potential of these derivatives. The computational methods employed, including molecular docking and MD simulations, rely on simplified representations of the binding environment. These models do not fully capture solvent effects, entropy, and the conformational flexibility of protein-ligand complexes, which could influence the accuracy of binding affinity predictions. Additionally, this study focused on a limited number of the synthesized derivatives (AMJ3, AMJ4, AMJ5, and AMJ6), restricting the scope for establishing a comprehensive structure-activity relationship. Expanding the derivative library in future research will provide deeper insights into the relationship between molecular structure and biological activity.

6 Conclusion

In conclusion, we have synthesized four novel compounds, (*E*)-2,4-dimethoxy-6-(4-methoxystyryl)benzaldehyde, which

contain resveratrol derivatives. These identified novel molecules were characterized and underwent a detailed mass spectral analysis. Molecular docking studies revealed that AMJ3 and AMJ6 exhibited significantly higher binding affinities and more stable interactions with the MDM2 protein compared to AMJ4 and AMJ5. Higher binding energies and interaction details suggest that AMJ3 and AMI6 may be potential MDM2 inhibitors for further development. This indicates that AMJ3 and AMJ6 molecules formed strong hydrogen bonds with key residues such as His75, Gln51, Leu33, and Phe34, which are important for efficient MDM2 inhibition. MD simulations confirmed the stability of the complexes formed by AMJ3 and AMJ6 with MDM2 over a 150 ns simulation period. AMJ3 demonstrated stable RMSD values after an initial equilibration phase, with minor fluctuations observed during specific intervals. Similarly, AMJ6 maintained stability after an initial equilibration phase, with consistent RMSD values throughout the simulation. In addition, RMSF analysis demonstrated low fluctuations at the site of binding, indicating that these interactions were stable. Therefore, our results indicate that AMJ3 and AJM6 are possible candidates to inhibit MDM2 protein in cancer therapy. Detailed insights from MD and docking studies offer a solid basis for the rational design of more potent anticancer agents targeting the MDM2 protein. Among the synthesized compounds, AMJ3 demonstrated the highest antiproliferative activity against HCT-116 cancer cells (IC₅₀: 22.69 \pm 2.47 µg/ mL) while maintaining high selectivity for normal WI-38 cells (IC₅₀: 75.86 \pm 2.73 μ g/mL). In MDM2-p53 inhibition assays, AMJ3 exhibited superior activity (IC₅₀: 0.24 ± 0.02 µM) compared to the reference compound Nutlin-3a (IC₅₀: $0.39 \pm 0.03 \mu M$). Similarly, AMJ5 displayed promising activity in both MTT assays and ELISA-based inhibition studies. Future work will include more biological experiments to validate these computational results and explore the therapeutic potential of these compounds in clinical settings.

Acknowledgment: The authors would like to extend their sincere appreciation to the Ongoing Research Funding Program (ORF-2025-189), King Saud University, Riyadh, Saudi Arabia.

Funding information: This work is financially supported by the Ongoing Research Funding Program (ORF-2025-189), King Saud University, Riyadh, Saudi Arabia.

Author contributions: Amjad Ibrahim Oraibi, Ashour H. Dawood, and Nawres Debbabi: conceptualization, original draft writing, reviewing, and editing; Leila Chekir-Ghedira,

Ali Majeed Ali Almukram, Khalid S. Almaary: formal analysis, investigations, funding acquisition, reviewing, and editing; and: Fakhreldeen Dabiellil and Soumaya Kilani-Jaziri: resources, data validation, data curation, and supervision.

Conflict of interest: The authors declare that they have no competing interests.

Ethical approval: The conducted research is not related to either human or animals use.

Data availability statement: All data generated or analysed during this study are included in this published article [and its supplementary information files].

References

- [1] Oraibi AI, Karav S, Khallouki F. Exploration of rosmarinic acid as anti-esophageal cancer potential by use of network pharmacology and molecular docking approaches. Atl J Life Sci. 2025;2025:11.
- [2] Bray F, Laversanne M, Sung H, Ferlay J, Siegel RL, Soerjomataram I, et al. Global cancer statistics 2022: GLOBOCAN estimates of incidence and mortality worldwide for 36 cancers in 185 countries. CA: Cancer J Clin. 2024;74:229–63.
- [3] Debela DT, Muzazu SG, Heraro KD, Ndalama MT, Mesele BW, Haile DC, et al. New approaches and procedures for cancer treatment: Current perspectives. SAGE Open Med. 2021;9:20503121211034366. doi: 10.1177/20503121211034366.
- [4] Manaithiya A, Alam O, Sharma V, Naim MJ, Mittal S, Azam F, et al. Current status of novel pyridine fused derivatives as anticancer agents: An insight into future perspectives and structure activity relationship (SAR). Curr Top Med Chem. 2021;21:2292–349.
- [5] Sun SY, Crago A. MDM2 implications for potential molecular pathogenic therapies of soft-tissue tumors. J Clin Med. 2023;12:3638.
- [6] Zafar A, Khan MJ, Naeem A. MDM2- an indispensable player in tumorigenesis. Mol Biol Rep. 2023;50:6871–83.
- [7] Yao Y, Zhang Q, Li Z, Zhang H. MDM2: Current research status and prospects of tumor treatment. Cancer Cell Int. 2024;24:1–13.
- [8] Henningsen KM, Manzini V, Magerhans A, Gerber S, Dobbelstein M. MDM2-driven ubiquitination rapidly removes p53 from its cognate promoters. Biomolecules. 2022;12:22.
- [9] Koo N, Sharma AK, Narayan S. Therapeutics targeting p53-MDM2 interaction to induce cancer cell death. Int J Mol Sci. 2022;23:5005.
- [10] Hernández Borrero LJ, El-Deiry WS. Tumor suppressor p53: Biology, signaling pathways, and therapeutic targeting. Biochim Biophys Acta Rev Cancer. 2021;1876:188556.
- [11] Fischer M, Sammons MA. Determinants of p53 DNA binding, gene regulation, and cell fate decisions. Cell Death Differ. 2024;31(7):836–43.
- [12] Nag S, Zhang X, Srivenugopal KS, Wang MH, Wang W, Zhang R. Targeting MDM2-p53 interaction for cancer therapy: Are we there yet? Curr Med Chem. 2014;21:553–74.

- [13] Wang H, Guo M, Wei H, Chen Y. Targeting p53 pathways: Mechanisms, structures, and advances in therapy. Signal Transduct Target Ther. 2023;8(1):92.
- [14] Brooks CL, Gu W. p53 ubiquitination: Mdm2 and beyond. Mol Cell. 2006;21:307–15.
- [15] Kumar S, Chang Y-C, Lai K-H, Hwang TL. Resveratrol, a molecule with anti-inflammatory and anti-cancer activities: Natural product to chemical synthesis. Curr Med Chem. 2021;28:3773–86.
- [16] Bohara RA, Tabassum N, Singh MP, Gigli G, Ragusa A, Leporatti S. Recent overview of resveratrol's beneficial effects and its nanodelivery systems. Molecules. 2022;27(16):5154.
- [17] Anwar MJ, Altaf A, Imran M, Amir M, Alsagaby SA, Abdulmonem WA, et al. Anti-cancer perspectives of resveratrol: a comprehensive review. Food Agric Immunol. 2023;34:2265686.
- [18] Mobashar A, Najam K, Akbar Z, Barkat K, Hussain K, Nadeem H, et al. Evaluation of anti-inflammatory and anti-arthritic activities of Benzimidazole derivative 2-((1H-benzo[d]imiadazol-2-yl) thio)-1-3, 5-diphenyl-1h-pyrazol-1-yl) ethanone. Atl | Life Sci. 2025;2025:8.
- [19] Pizzorno A, Dubois J, Machado D, Cartet G, Traversier A, Julien T, et al. Influenza A viruses alter the stability and antiviral contribution of host E3-ubiquitin ligase Mdm2 during the time-course of infection. Sci Rep. 2018;8(1):3746.
- [20] Marcellino BK, Hoffman R, Tripodi J, Lu M, Kosiorek H, Mascarenhas J, et al. Advanced forms of MPNs are accompanied by chromosomal abnormalities that lead to dysregulation of TP53. Blood Adv. 2018;2:3581–9.
- [21] Shen H, Maki CG. Pharmacologic activation of p53 by small-molecule MDM2 antagonists. Curr Pharm Des. 2011;17:560–8.
- [22] Amarakoon D, Lee WJ, Tamia G, Lee SH. Indole-3-carbinol: Occurrence, health-beneficial properties, and cellular/molecular mechanisms. Annu Rev Food Sci Technol. 2023;14:347–66.
- [23] Bauer S, Demetri GD, Halilovic E, Dummer R, Meille C, Tan D, et al. Pharmacokinetic–pharmacodynamic guided optimisation of dose and schedule of CGM097, an HDM2 inhibitor, in preclinical and clinical studies. Br J Cancer. 2021;125:687–98.
- [24] Patnaik A, Tolcher A, Beeram M, Nemunaitis J, Weiss GJ, Bhalla K, et al. Clinical pharmacology characterization of RG7112, an MDM2 antagonist, in patients with advanced solid tumors. Cancer Chemother Pharmacol. 2015;76:587–95.
- [25] Zhang M, Chen XY, Dong XD, Wang JQ, Feng W, Teng QX, et al. NVP-CGM097, an HDM2 inhibitor, antagonizes ATP-binding cassette subfamily B member 1-mediated drug resistance. Front Oncol. 2020;10:1219. doi: 10.3389/FONC.2020.01219.
- [26] McKean M, Tolcher AW, Reeves JA, Chmielowski B, Shaheen MF, Beck JT, et al. Newly updated activity results of alrizomadlin (APG-115), a novel MDM2/p53 inhibitor, plus pembrolizumab: Phase 2 study in adults and children with various solid tumors. J Clin Oncol. 2022;40:9517.
- [27] Vuaroqueaux V, Hendriks HR, Al-Hasani H, Peille AL, Das S, Fiebig HH. Pharmacogenomics characterization of the MDM2 inhibitor MI-773 reveals candidate tumours and predictive biomarkers. NPJ Precis Oncol. 2021;5:1–11.
- [28] Gungordu S, Aptullahoglu E. Targeting MDM2-mediated suppression of p53 with idasanutlin: a promising therapeutic approach for acute lymphoblastic leukemia. Invest N Drugs. 2024;42(6):603–11.
- [29] Sahin I, Zhang S, Navaraj A, Zhou L, Dizon D, Safran H, et al. AMG-232 sensitizes high MDM2-expressing tumor cells to T-cell-mediated killing. Cell Death Discov. 2020;6(1):57.

- [30] Fiolek TJ, Keel KL, Tepe JJ. Fluspirilene analogs activate the 20S proteasome and overcome proteasome impairment by intrinsically disordered protein oligomers. ACS Chem Neurosci. 2021;12:1438–48.
- [31] Steele TS, Brunson JK, Maeno Y, Terada R, Allen AE, Yotsu-Yamashita M, et al. Domoic acid biosynthesis in the red alga Chondria armata suggests a complex evolutionary history for toxin production. Proc Natl Acad Sci. 2022;119(6):e2117407119.
- [32] Halgren TA, Murphy RB, Friesner RA, Beard HS, Frye LL, Pollard WT, et al. Glide: A new approach for rapid, accurate docking and scoring. 2. Enrichment factors in database screening. J Med Chem. 2004;47:1750–9.
- [33] Harder E, Damm W, Maple J, Wu C, Reboul M, Xiang JY, et al. OPLS3: A force field providing broad coverage of drug-like small molecules and proteins. J Chem Theory Comput. 2016;12:281–96.

- [34] Salmaso V, Moro S. Bridging molecular docking to molecular dynamics in exploring ligand-protein recognition process: An overview. Front Pharmacol. 2018;9:393738.
- [35] Manaithiya A, Bhowmik R, Acharjee S, Sharma S, Kumar S, Imran M, et al. Elucidating molecular mechanism and chemical space of chalcones through biological networks and machine learning approaches. Comput Struct Biotechnol J. 2024;23:2811–36.
- [36] Shivakumar D, Harder E, Damm W, Friesner RA, Sherman W. Improving the prediction of absolute solvation free energies using the next generation opls force field. J Chem Theory Comput. 2012;8:2553–8.
- [37] Mark P, Nilsson L. Structure and dynamics of the TIP3P, SPC, and SPC/E water models at 298 K. J Phys Chem A. 2001;105:9954–60.